Charged-Current Neutrino-Induced Single-Pion Production in the Superscaling Approach and the Relativistic Distorted-Wave Impulse Approximation

Jesus Gonzalez-Rosa , Alexis Nikolakopoulos , Maria B. Barbaro , Juan A. Caballero , Raúl González-Jiménez , Guillermo D. Megias *

Posted Date: 24 February 2026

doi: 10.20944/preprints202602.1441.v1

Keywords: neutrino interactions; electroweak interactions; nuclear matter; scaling; relativistic mean field; pion production; neutrino oscillation; inelastic scattering; nucleon resonance

Article

Charged-Current Neutrino-Induced Single-Pion Production in the Superscaling Approach and the Relativistic Distorted-Wave Impulse Approximation

Jesus Gonzalez-Rosa [1], Alexis Nikolakopoulos [2], Maria B. Barbaro [3], Juan A. Caballero [1], Raúl González-Jiménez [1] and Guillermo D. Megias [1,*]

[1] Departamento de Física Atómica, Molecular y Nuclear, Universidad de Sevilla, 41080 Sevilla, Spain
[2] Physics Department, University of Washington, Seattle WA, USA
[3] INFN, Sezione di Torino, Via P. Giuria 1, 10125 Torino, Italy
* Correspondence: megias@us.es

Abstract

In this work, we present a detailed comparison of the SuSAv2 (SuperScaling Approach version 2) and RDWIA (Relativistic Distorted-Wave Impulse Approximation) models with measurements of charged-current neutrino-induced single-pion production from different experiments (T2K, MINERvA and MiniBooNE), studying the differences between the two theoretical descriptions. The neutrino energy range in these experiments spans from hundreds of MeV to roughly 20 GeV, and the nuclear targets are mainly composed of ^{12}C. The SuSAv2 model uses the single-nucleon inelastic structure functions from the ANL-Osaka DCC model, which allows for a separation of pion production channels, distinguishing between the π^+, π^- and π^0 final states. In the RDWIA approach, the Hybrid model developed by the Ghent group is used for the description of the boson-pion-nucleon vertex.

Keywords: neutrino interactions; electroweak interactions; nuclear matter; scaling; relativistic mean field; pion production; neutrino oscillation; inelastic scattering; nucleon resonance

1. Introduction

Neutrino oscillation experiments constitute a fundamental tool for exploring the properties of neutrinos, such as the possible violation of charge-parity symmetry or their mass hierarchy [1–3]. The interaction of the neutrino with the nucleus is a key piece in the reconstruction of the neutrino energy in oscillation experiments, a fundamental step in the determination of neutrino oscillation parameters and a source of major uncertainties in the analysis. As such, multiple theoretical and experimental efforts have been developed for this purpose. In these experiments, multiple channels are involved. For example, in the neutrino energy range of hundreds of MeV to a few GeV, the dominant interaction of the neutrino with the nucleus is the quasielastic (QE) process in which a single nucleon is knocked-out from the nucleus. In spite of this process being heavily relevant in the few GeV region, in experimental inclusive analyses, where all reaction channels are considered, other processes also give crucial contributions to the cross section, like two-particle two-hole interaction, the excitation of the nucleonic resonances, or deep-inelastic scattering (DIS). Hence, a reduction in the nuclear-medium uncertainties associated with all these processes, including neutrino-induced pion production, is needed to improve cross-section measurements and neutrino oscillation analyses.

Most experiments – MiniBooNE [4], MicroBooNE [5], T2K [6], MINERvA[7], NOνA [8] and future ones like HyperK [9] or DUNE [10] – operate on different energy ranges, such as 0.5-1 GeV (MicroBooNE, T2K, MiniBooNE) or around 10 GeV (DUNE, ArgoNEUT[11]). The importance of each channel depends on the energy in which the experiment operates: quasielastic scattering dominates at a neutrino energy of $0.5 - 1$ GeV, while pion production and other inelastic processes become dominant at higher energies. Diverse experimental efforts have been devoted to the study of these different

 doi:10.20944/preprints202602.1441.v1

reaction mechanisms. This is the case of charged-current neutrino interactions with only one pion detected in the final state of the process, together with the scattered lepton. These so-called CC1π events can be modeled as the excitation of a nucleonic resonance followed by its decay into nucleons, pions and other mesons, non-resonant pion production processes or intranuclear pion rescattering effects. These studies also allow us to compare and validate theoretical models for the description of neutrino-induced pion production.

On the theoretical side, several groups [12–22] have studied neutrino-induced pion production on nuclei, providing different descriptions of the initial nuclear state, the pion production from a bound nucleon, and the subsequent pion-nucleon interaction within the residual nucleus. Most of the initial studies were based on Fermi gas approaches of non-interacting nucleons [23,24], but recently more sophisticated descriptions have been developed, incorporating Random Phase Approximation (RPA) calculations [18,25], the plane-wave impulse approximation (PWIA) together with the use of realistic spectral functions [26] or relativistic distorted-wave impulse approximation (RDWIA) approaches [27].

All previous nuclear models describing lepton-induced single-pion production (SPP) on the nucleus are based on the impulse approximation, i.e., they consider that the virtual boson couples only one nucleon in the nucleus. The description of the elementary boson-nucleon-pion vertex is done differently depending on the model considered. For example, the Hybrid model [28–30] is used in the RDWIA approach [31], and the ANL-Osaka Dynamical Coupled-Channels model [32–36] (DCC in what follows) has been recently implemented in the SuSAv2 framework [37]. The DCC has also been used in the extended factorization scheme [26], which was incorporated in the ACHILLES event generator [38]; the Hybrid was implemented in the NuWro event generator using a local Fermi gas as nuclear model [22]. A different approach for neutrino-induced single pion production is the MK model [39], which is used in the NEUT event generator [40].

In a recent work [37,41], the superscaling model SuSAv2, developed for the charged-current quasielastic neutrino-nucleus cross section, was extended to the full inelastic regime (SuSAv2-inelastic model). In this framework, the DCC model has been implemented [37] to give an accurate description of neutrino-induced one- and two-pion production, among other meson-production mechanisms in the resonance region. This model has been widely tested for photon, electron and neutrino scattering off single nucleons, providing information about the single-nucleon inelastic structure functions (W_{1-5}) [32–36]. This model accounts for the structure functions associated with the whole inclusive contribution and also the functions connected to lepton-induced SPP. In what follows, we refer to them as inclusive-DCC and π-DCC, respectively. The inclusive-DCC takes into account two- and three-body meson-baryon final states (πN, ηN, $K\Lambda$, $K\Sigma$ and $\pi\pi N$) in a couple channel approach, while the π-DCC accounts only for a particular SPP channel. Then, using π-DCC inelastic structure functions, we can distinguish between channels with a single π^+, π^0, or π^- in the final state.

The Hybrid model, presented in [29], aims at describing lepton-induced SPP in a broader energy region, so it could be used without phase-space restrictions in neutrino-oscillation experiments. It is based on the low-energy model of [28] and a high-energy Regge-based model, and can be used for SPP induced by electrons and charged- and neutral-current neutrinos. The Hybrid model was later incorporated in the RDWIA nuclear framework, so it could be used to model cross sections for incoherent SPP on the nucleus [21,30,31,42]. It has been compared to MiniBooNE, MINERvA and T2K pion-detected cross section data. The tension observed in these studies between bubble-chamber and MINERvA data was shown in [31], using the RDWIA and also comparing with the relativistic plane-wave impulse-approximation (RPWIA).

All these approaches are described in Sect. 2, where the theoretical formalisms for the SuSAv2-inelastic and RDWIA frameworks are summarized. In Sect. 3, we show the comparison between the predictions of the different theoretical models and the CC1π experimental data provided by MiniBooNE (Sect. 3.0.1), MINERvA (Sect. 3.0.2) and T2K (Sect. 3.0.3), that operate at diverse kinematics and with different targets. In Sect. 4, we draw our conclusions.

 doi:10.20944/preprints202602.1441.v1

2. Formalism

The superscaling approach (SuSA) is based on the scaling properties exhibited by inclusive electron scattering where the QE scattering cross section can be written, under certain conditions, as a term containing the single-nucleon cross section times a scaling function (f) that embodies the nuclear dynamics. The analysis of inclusive electron scattering data [43] has shown that for transferred momentum (q) values around 300 MeV/c or higher, the scaling function does not depend on q (scaling of 1st kind) nor on the nuclear species (scaling of 2nd kind) and can therefore be expressed in terms of a single variable ψ, the so-called scaling variable. A more detailed description of superscaling can be found in [43–50]. This approach has also been successfully applied to inclusive charged-current quasielastic (CCQE) neutrino scattering and, most recently, to the full inelastic regime for both electron and neutrino reactions. The corresponding model for the quasielastic region (SuSAv2-QE) is based on a set of QE scaling functions extracted from the relativistic mean field (RMF) theory [51].

The SuSAv2-inelastic model is an extension of the SuSAv2-QE approach to the inelastic regime [52, 53]. The double differential cross section for lepton-nucleus scattering with respect to the transferred energy ω and the scattered lepton solid angle Ω can be written in the general form [44]

$$\frac{d\sigma}{d\Omega d\omega} = \sigma_0 \sum_K v_K R^K \,, \tag{1}$$

where σ_0 is an elementary cross section (the Mott cross section in the case of electron scattering), v_K are lepton kinematic Rosenbluth factors and R^K are the nuclear response functions, containing all the information about nuclear dynamics and the inner nucleon structure functions. The summed index K is associated to different components of the nuclear tensor with respect to the direction of the transferred momentum $\mathbf{q}$.

The inclusive nuclear responses, after integrating over the possible values of the invariant mass W_X of the hadronic final states, depend only on the energy and momentum transferred to the nucleus.

The invariant mass for lepton-nucleus reactions, W_X, can be determined via the 4-momentum of the final hadronic system P_X, which is defined by 4-momentum conservation as:

$$k_i + P_A = k_f + P_{A-1} + P_X \,, \tag{2}$$

where k_i and k_f are the initial and final leptons 4-momenta, and P_A and P_{A-1} are the 4-momenta of the target and residual nucleus, respectively. Hence,

$$W_X^2 = P_X^2 \,. \tag{3}$$

In the case of the SPP on nucleons, one has

$$W_X^2 = (P_N + P_\pi)^2 = (Q + P_i)^2 = P_X^2 \,, \tag{4}$$

being P_N, P_π and P_i the 4-momentum of the final nucleon, produced pion and initial nucleon, respectively.

In the SuSAv2-inelastic model [37,41,52,53], the nuclear responses are given by

$$R_K^{inel}(q,\omega) = N \frac{2T_F m_N^3}{k_F^3 q} \times \int_{\mu_X^{min}}^{\mu_X^{max}} d\mu_X \mu_X f^{model}(\psi_X) G_K^{inel}(q,\omega,W_X) \,, \tag{5}$$

being $\mu_X \equiv W_X/m_N$ the dimensionless invariant mass, N the number of nucleons from the target involved in the reaction, k_F the Fermi momentum and $T_F \equiv \sqrt{m_N^2 + k_F^2} - m_N$ the Fermi kinetic energy. Thus, the inelastic nuclear responses are defined as the integral over all possible final hadronic states

 doi:10.20944/preprints202602.1441.v1

of the single-nucleon inelastic hadronic tensor G_K^{inel} (characterized by the inelastic structure functions W_{1-5}) times the inelastic scaling function f^{model} evaluated in a given nuclear model. The latter is written in terms of $\psi_X \equiv \psi_X(q, \omega, W_X)$, which is the extension of the QE scaling variable ψ to the inelastic regime and now depends on the final state invariant mass W_X. The limits of the integral ($\mu_X^{min/max}$) can be adjusted depending on the kinematics considered for a particular experimental or theoretical analysis and the limitations of the single-nucleon model used to characterize the hadronic tensor. For example, in the case of the DCC model, there is a limitation up to an invariant mass of 2.1 GeV and Q^2 below 3 GeV^2 [32]. In general, the limits of this integral either in the SuSAv2 model or in a RFG framework can be defined as $\mu_X^{min} = 1 + m_\pi/m_N$ and $\mu_X^{max} = 1 + \omega/m_N - E_S$, being m_π the pion mass and E_S the separation energy for a bound nucleon [54].

In Figure 1, we show the single-nucleon structure functions of the DCC model, displaying both π-DCC and inclusive-DCC contributions. As expected, both curves match below the two-pion production threshold, in the region dominated by the Δ resonance, but as the invariant mass increases, the single-pion results (π-DCC) are below the inclusive ones that also take into account effects beyond SPP as mentioned above.

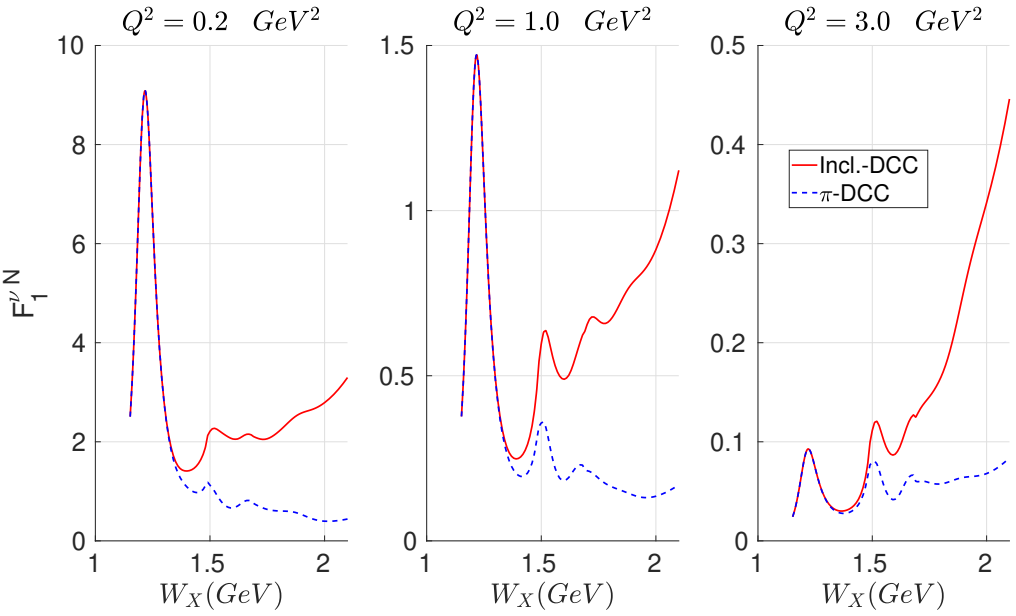

Figure 1. Inclusive-DCC (red continuous line) and π-DCC (blue dashed line) inelastic structure functions $F_1 = m_N W_1$ for neutrinos as a function of the invariant mass at different values of Q^2, namely 0.2 (left), 1 (center) and 3 (right) GeV^2.

In Figure 1, we show the single-nucleon structure functions of the DCC model, displaying both π-DCC and inclusive-DCC contributions. As expected, both curves match below the two-pion production threshold, in the region dominated by the Δ resonance, but as the invariant mass increases, the single-pion results (π-DCC) are below the inclusive ones that also take into account effects beyond SPP as mentioned above.

Unlike the SuSAv2 model, in the RDWIA approach, the cross section describing the SPP process gives information not only about final-state leptons but also about final-state hadrons (pion and nucleon). It reads [27]:

$$\frac{d^8\sigma}{dE_f d\Omega_f dE_\pi d\Omega_\pi d\Omega_N} = \mathcal{F} \frac{k_f E_f p_N^2 E_\pi k_\pi}{(2\pi)^8 f_{rec}} l_{\mu\nu} h^{\mu\nu} \,, \tag{6}$$

where

$$f_{rec} = \frac{p_N}{E_N} \left(1 + \frac{E_N}{E_{A-1}} \left| 1 + \frac{\mathbf{p}_N \cdot (\mathbf{k}_\pi - \mathbf{q})}{p_N^2} \right| \right) . \tag{7}$$

 doi:10.20944/preprints202602.1441.v1

This expression is valid for SPP induced by electromagnetic as well as weak-neutral and weak-charged current interactions. It is written in terms of the lepton, outgoing pion and outgoing nucleon variables. The factor $\mathcal{F}$ depends on the particular process under study and includes the boson propagator and the coupling constants at the leptonic vertex. The expression involves the leptonic tensor ($l_{\mu\nu}$) and the hadronic tensor ($h^{\mu\nu}$).

The hadronic tensor is defined as

$$h^{\mu\nu} = \sum_{\kappa} \sum_{m_j, s_N} [J^{\mu}(\kappa, m_j, s_N)]^* J^{\nu}(\kappa, m_j, s_N)\,. \tag{8}$$

The outer sum runs over bound states labelled by κ. The total angular momentum of the bound state is $j = |\kappa| - 1/2$ and the orbital angular momentum is $l = j \pm 1/2$ for $\kappa = \pm|\kappa|$. Here m_j is the third component of the angular momentum, and s_N is associated with the spin projection of the outgoing nucleon. We have suppressed here and in the following the explicit dependence on the four-momenta of the exchanged boson, the nucleon and the pion. The tensor is written in terms of the matrix elements of the hadronic current (J^{μ}), which can be expressed as the Fourier transform of a current density

$$J^{\mu}(\kappa, m_j, s_N) = \int \mathrm{d}^3\mathbf{r} e^{i\mathbf{q}\cdot\mathbf{r}} \mathcal{J}^{\mu}(\mathbf{r}, \kappa, m_j, s_N). \tag{9}$$

In the relativistic impulse approximation it has the following structure

$$\mathcal{J}^{\mu}(\mathbf{r}) \sim \phi^*_{\pi}(\mathbf{r}) \bar{\psi}_N(\mathbf{r}, s_N) \hat{\mathcal{O}}^{\mu}_{1\pi} \psi(\mathbf{r}, \kappa, m_j)\,. \tag{10}$$

Here ψ_N and ψ are, respectively, scattering and bound-state nucleon wavefunctions represented by four-component spinors, ϕ_{π} is the pion wavefunction, and $\hat{\mathcal{O}}_{1\pi}$ is a bilinear operator. More details of the spinors and the operator can be found in [29–31]. In particular, the calculations for charged pion production presented here are identical to those of [31], and π^0 production results were included in [55].

Results in this work are obtained using the following approximations: the pion is treated as a plane wave, and the 'local approximation' is invoked. The latter means that momenta that enter in the operator are fixed to their asymptotic values. With these approximations the calculation of the current simplifies as explained in [31]. Recently, results without the local approximation and an analysis of the effects of invoking it were presented in [21]. The outgoing nucleon wavefunctions are obtained with the energy-dependent RMF (EDRMF) potential from [27]. In this approach, initial and final state potentials are identical for low nucleon energies, which leads naturally to Pauli blocking, and the conservation of the Dirac current. At higher nucleon kinetic energies the potentials soften, thereby avoiding unsound behavior caused by using an energy-independent potential [56].

In the following section, we compare the predictions of the models described above for charged-current neutrino- and antineutrino-induced SPP off the nucleon and on the nucleus.

3. Results

In this section, we compare the predictions of the SuSAv2-DCC and EDRMF-Hybrid models with data on charged current neutrino-induced SPP. Our analysis focuses on channels that result in a single pion in the final state, where a significant contribution arises from the Δ resonance. The SuSAv2-inelastic model with π-DCC structure functions allows to separate the different SPP channels, i.e., π^+, π^0, or π^-. Similarly, the SPP channels are computed separately in the EDRMF-Hybrid model.

Before comparison to nuclear target data, we present in Figure 2, the total cross sections for SPP off the nucleon for all neutrino and antineutrino channels obtained from the Hybrid and DCC models. For $W_X < 1.4$ GeV, where the main contribution comes from the Δ resonance, the prediction of the DCC model is higher than that of the Hybrid model, except for the π^0 channel. On the other hand, without this limitation in the invariant mass, the Hybrid model predicts larger total cross sections with the exception of the π^+ channel.

 doi:10.20944/preprints202602.1441.v1

In Tables 1 and 2, the flux-folded CC1π total cross sections for the different experiments are shown. We consider both neutrino and antineutrino fluxes for MINERvA and the neutrino fluxes for T2K and MiniBooNE to analyze the flux-folded total cross sections for different neutrino- and antineutrino-induced SPP off free nucleons. This table shows the cross sections for $W_X < 1.4$ GeV, where the Δ resonance dominates, and for $W_X < 1.8$ GeV, which is a common threshold used in the MINERνA analyses. In the case of MINERνA, we generally observe a notable difference between the total cross section from the DCC and Hybrid models, matching the differences shown in Figure 2 at higher energies. For T2K and MiniBooNE, the models differ significantly for neutrino-induced π^+ production, which is also observed at energies around and below 1 GeV in the curves of Figure 2 for that particular channel. The models tend to be more similar for the other pion production channels.

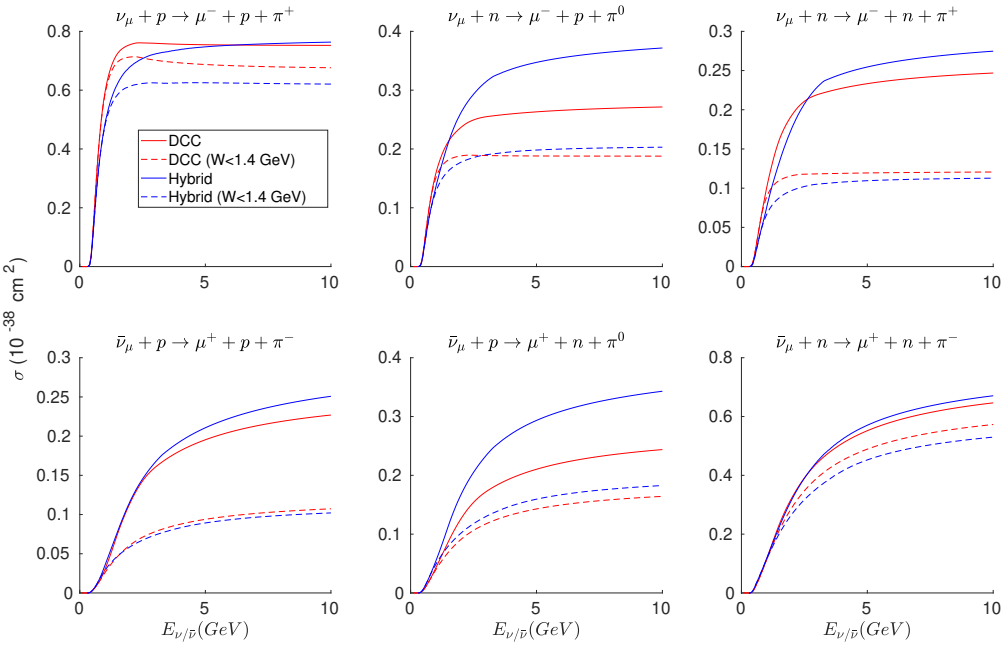

Figure 2. CC1π total cross sections ($10^{-38} cm^2$) in terms of the neutrino (top) or antineutrino (bottom) energies for different pion production channels: (top left) $p \to p + \pi^+$, (top center) $n \to p + \pi^0$, (top right) $n \to n + \pi^+$, (bottom left) $p \to p + \pi^-$, (bottom center) $p \to n + \pi^0$ and (bottom right) $n \to n + \pi^-$. Results from DCC and Hybrid models are shown, also considering a threshold of 1.4 GeV in the invariant mass.

Table 1. Flux-folded CC1π total cross sections (10^{-40}cm^2) for neutrino scattering on single nucleons and considering $W_X < 1.4$ GeV and W_X <1.8 GeV, respectively. The kinematics of MINERvA, T2K and MiniBooNE considering their respective neutrino fluxes are analyzed comparing DCC and Hybrid results.

	MINERvA ν flux		T2K ν flux		MiniBooNE ν flux	
	W_X <1.4 GeV	W_X <1.8 GeV	W_X <1.4 GeV	W_X <1.8 GeV	W_X <1.4 GeV	W_X <1.8 GeV
$\nu p\pi^+$(DCC)	69.03	74.69	30.40	31.02	39.22	39.98
$\nu p\pi^+$(Hybrid)	62.12	72.03	24.9	25.72	33.5	34.5
$\nu n\pi^0$(DCC)	18.61	25.04	7.95	8.64	10.18	11.01
$\nu n\pi^0$(Hybrid)	18.97	31.33	6.75	7.77	9.05	10.32
$\nu n\pi^+$(DCC)	11.66	21.54	4.52	5.60	5.92	7.25
$\nu n\pi^+$(Hybrid)	10.46	22.53	3.38	4.39	4.67	5.93

In the following subsections, we show the comparison between the SuSAv2 π-DCC and the EDRMF-Hybrid predictions and with CC1π neutrino-nucleus data.

 doi:10.20944/preprints202602.1441.v1

Table 2. Flux-folded CC1π total cross sections (10^{-40}cm^2) for antineutrino scattering on single nucleons and considering W_X < 1.4 GeV and W_X <1.8 GeV, respectively. The kinematics of MINERvA considering the antineutrino flux are analyzed comparing DCC and Hybrid results.

	MINERvA $\bar{\nu}$ flux	
	W_X <1.4 GeV	W_X <1.8 GeV
$\bar{\nu}p\pi^-$(DCC)	7.76	15.72
$\bar{\nu}p\pi^-$(Hybrid)	7.46	16.69
$\bar{\nu}p\pi^0$(DCC)	11.70	16.99
$\bar{\nu}p\pi^0$(Hybrid)	13.16	23.44
$\bar{\nu}n\pi^-$(DCC)	39.0	43.92
$\bar{\nu}n\pi^-$(Hybrid)	36.19	45.03

3.0.1. MiniBooNE

The MiniBooNE experiment uses mineral oil, CH_2, as a target. Figure 3 shows the associated neutrino flux for CC1π studies. The flux ranges from 0 to 3 GeV, although only values between 0.5 and 2 GeV are considered for the experimental analyses [57,58]. The flux peaks around $E_\nu \sim 0.5$ GeV.

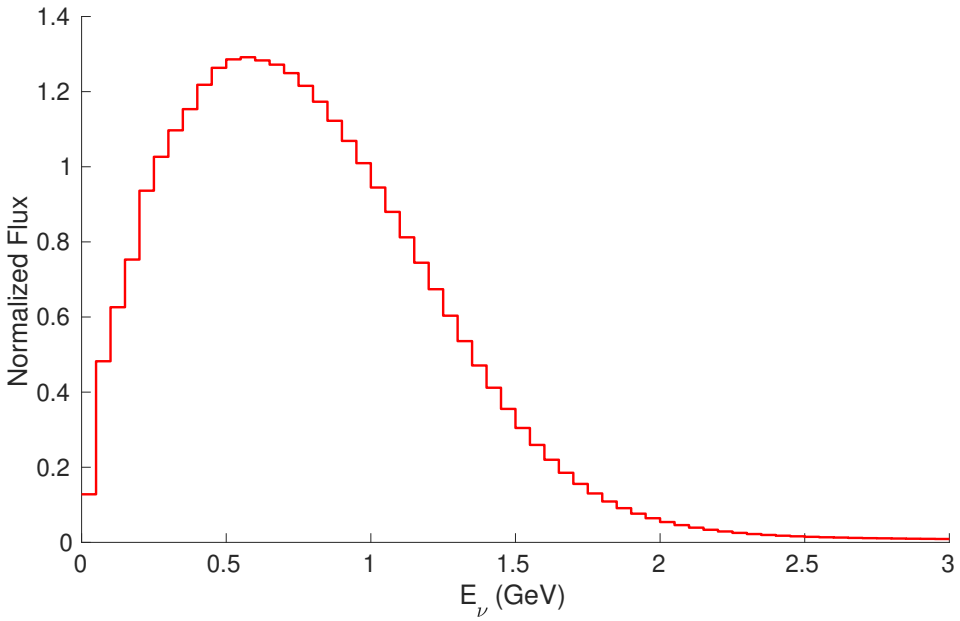

Figure 3. Normalized neutrino flux from MiniBooNE [57,58] for neutrino-induced pion production processes.

Figure 4 presents the CC1π^0 single-differential cross sections as a function of the muon momentum and the cosine of the muon scattering angle. In this channel, both the final-state muon and π^0 are detected. The SuSAv2 π-DCC model in general underestimates the data. The model prediction does not include coherent pion production, though according to [18] its contribution is negligible in this case. In a similar way, intra-nuclear cascade effects (e.g., a π^+ converting into a π^0), are not included in the model which can explain part of the observed underestimation [30,59] Another reason for this discrepancy can be related to the difference between DCC and Hybrid, producing the latter larger results for CC1π^0, unlike other channels, as observed in Figure 2. However, at the relatively low energies of MiniBooNE, the differences between DCC and Hybrid are not expected to be as significant as for other higher-energy experiments, such as MINERvA, as will be discussed later. In general, the contribution given by SuSAv2 π-DCC accounts for roughly half of the total observed CC1π^0 MiniBooNE result.

The following figures (Figures 5–8) show results for CC1π^+ cross sections as a function of the muon kinetic energy, using the same flux shown in Figure 3. In this case there is an experimental cut in the phase space, so only processes with W^{exp} < 1.35 GeV are considered, being $W^{exp} \equiv$

 doi:10.20944/preprints202602.1441.v1

$\sqrt{m_N^2 + 2m_N\omega - |Q^2|}$. In Figure 5, the single-differential cross section is presented. Here, various pion production channels contribute, namely π^+ production from neutrino interactions with both neutrons and protons from carbon. The contribution of protons from the hydrogen component (H_2) of the target is also considered. The DCC model accounts for most of the cross section strength, but contributions from coherent and pion rescattering processes are missing. On the other hand, the EDRMF-Hybrid results are similar at these kinematics to the SuSAv2-DCC ones, being the latter approximately 5% higher, which is consistent with the results in Figure 2.

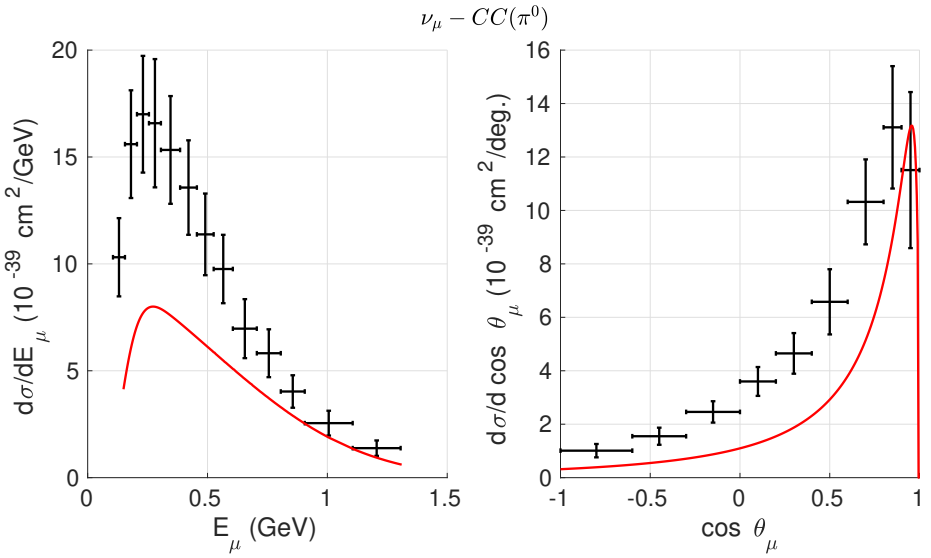

Figure 4. MiniBooNE flux-averaged CC1π^0 ν_μ-CH_2 differential cross sections as a function of the muon energy (left) and the cosine of the scattering angle (right) compared with SuSAv2 π-DCC. The flux is defined from 0.5 $< E_\nu$/GeV < 2. The experimental MiniBooNE points are taken from [58].

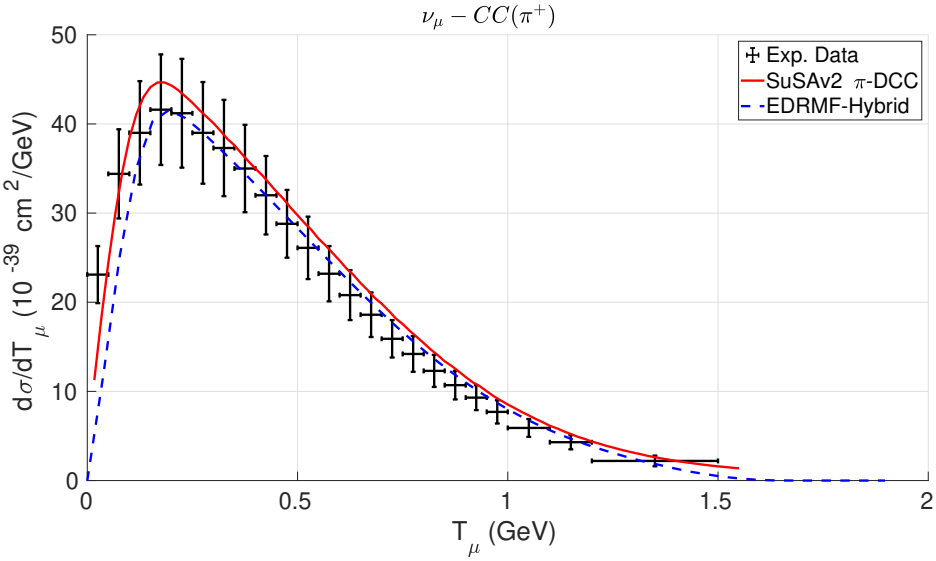

Figure 5. MiniBooNE flux-averaged CC1π^+ ν_μ-CH_2 differential cross section as a function of the muon kinetic energy compared with SuSAv2 π-DCC and EDRMF-Hybrid. The flux is defined from 0.5 $< E_\nu$/GeV < 2 and $W^{exp} < 1.35$ GeV. The MiniBooNE data are from [57].

Figure 6 shows the double-differential cross section in the very forward angular region. At low muon kinetic energies, the absence of the additional coherent and pion rescattering effects could lead to a more pronounced underestimation of the data [18]. These discrepancies between theory and data diminish as the muon kinetic energy increases, observing a good agreement with data for the EDRMF model at large T_μ values and a slight overestimation when compared with SuSAv2.

 doi:10.20944/preprints202602.1441.v1

In Figures 7 and 8, we present the charged-current single π^+ (CC1π^+) double-differential cross section as a function of the cosine of the muon scattering angle, averaged over bins of muon kinetic energy. In general, we observe good agreement with data for both models except at very forward angles and low-intermediate T_μ where the models underestimate the data; at large T_μ the data are overestimated. The agreement with data is slightly better for the EDRMF-Hybrid.

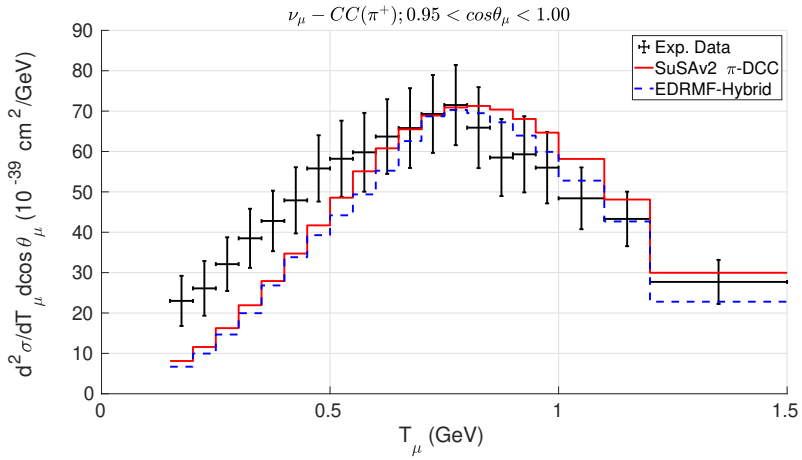

Figure 6. MiniBooNE flux-averaged CC1π^+ ν_μ-CH_2 double-differential cross sections for $0.95 < \cos\theta < 1$ as a function of the muon kinetic energy compared with SuSAv2 π-DCC and EDRMF-Hybrid. The flux is defined from $0.5 < E_\nu/\text{GeV} < 2$ and $W^{exp} < 1.35$ GeV. The experimental MiniBooNE points are taken from [57].

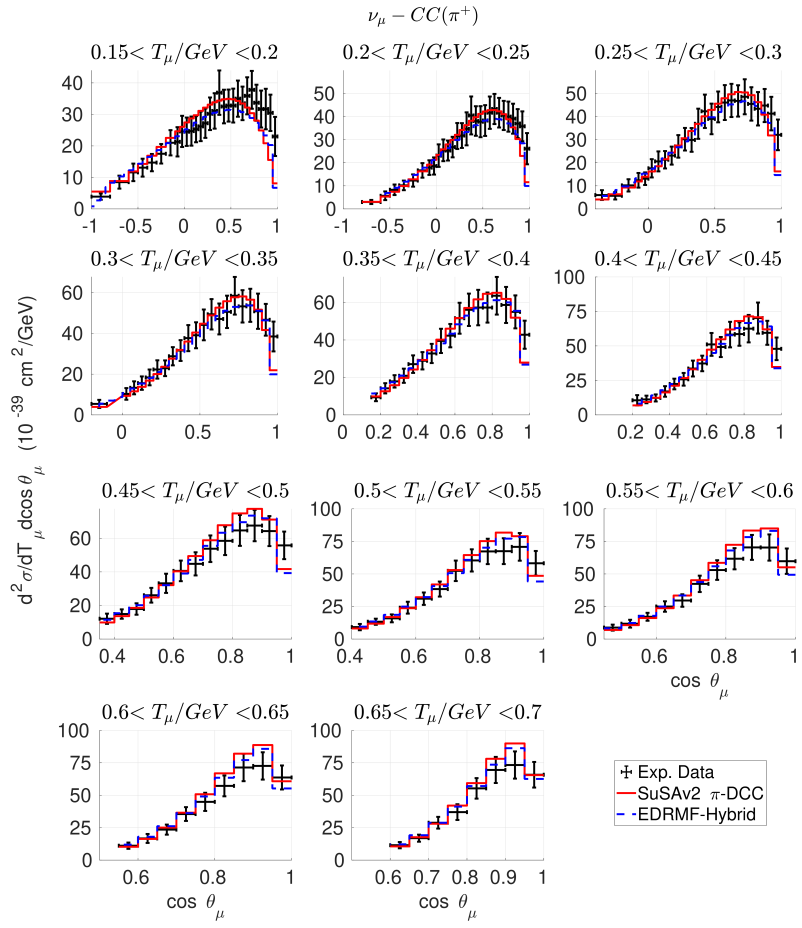

Figure 7. MiniBooNE flux-averaged CC1π^+ ν_μ-CH_2 double-differential cross sections for several values of muon kinetic energy as a function of the muon scattering angle. Data are compared with the SuSAv2 π-DCC and EDRMF-Hybrid. The flux is defined from $0.5 < E_\nu/\text{GeV} < 2$ and $W^{exp} < 1.35$ GeV. The MiniBooNE data are from [57].

Preprints.org (www.preprints.org) | NOT PEER-REVIEWED | Posted: 24 February 2026 doi:10.20944/preprints202602.1441.v1

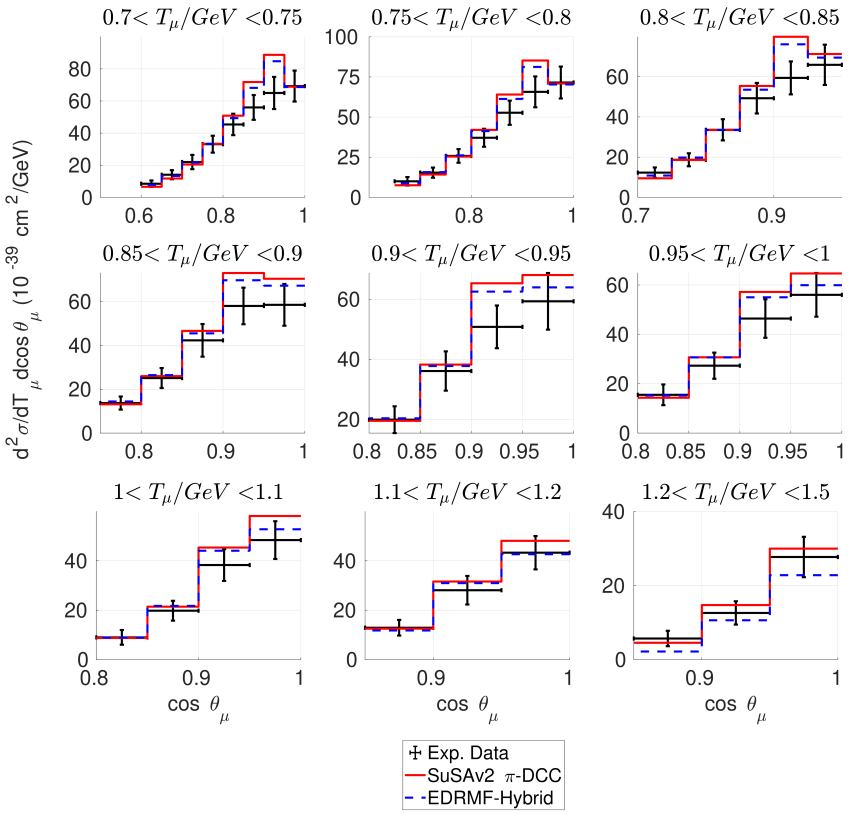

Figure 8. MiniBooNE flux-averaged CC1π^+ ν_μ-CH_2 double-differential cross sections for several values of muon kinetic energy as a function of the muon scattering angle compared with SuSAv2 π-DCC and EDRMF-Hybrid. The flux is defined from $0.5 < E_\nu/\text{GeV} < 2$ and $W^{exp} < 1.35$ GeV. The experimental MiniBooNE points are taken from [57].

3.0.2. MINERvA

In this experiment, the target material is hydrocarbon (CH). As shown in Figure 9, the flux for the different pion production channels peaks at approximately 3.5 GeV and extends up to 20 GeV, although it becomes negligible above 7 GeV. This energy range is significantly larger than that of the MiniBooNE experiment discussed previously.

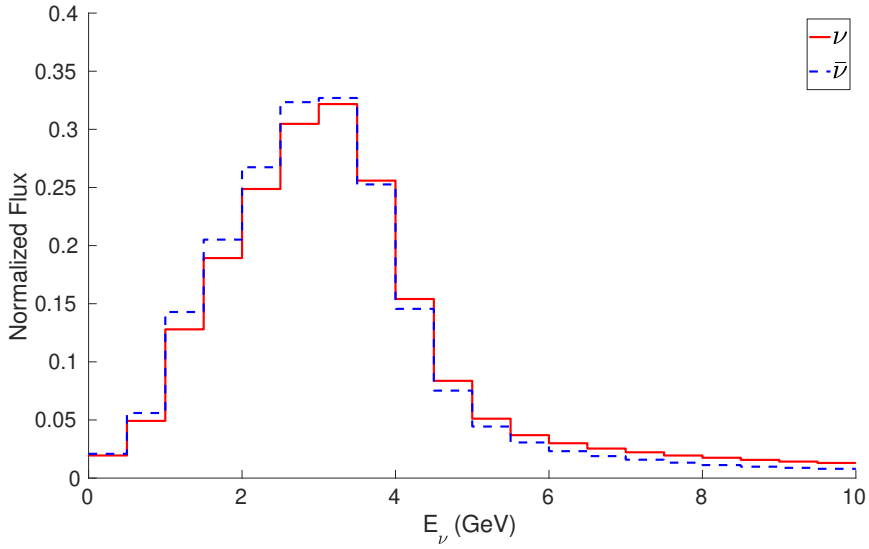

Figure 9. Normalized neutrino (red line) and antineutrino (blue dashed line) fluxes from MINERvA [60–62] for neutrino-induced pion production processes.

 doi:10.20944/preprints202602.1441.v1

In Figure 10, the MINERvA flux-folded CC1π single-differential cross sections in terms of the muon momentum and scattering angle for different neutrino- and antineutrino-induced pion production reactions on single-nucleons are analyzed to compare differences between DCC and Hybrid before including these approached in the corresponding nuclear models. We observe larger cross sections for DCC in the π^+ case, while for the π^- and π^0 channels the Hybrid provides larger results. These analyses are useful to understand the following results, when the models are compared with data for pion production on the nucleus. Note that for the results shown in Figure 10 and in Figures 11, 12 and 13, we have considered the following experimental restrictions: for π^+, $1.5 < E_\nu/\text{GeV} < 10$ and $W^{exp} < 1.4$ GeV; for antineutrino π^0, $1.5 < E_\nu/\text{GeV} < 10$ and $W^{exp} < 1.8$ GeV; for neutrino π^0, $1.5 < E_\nu/\text{GeV} < 20$, $\theta_\mu < 25$ deg. and $W^{exp} < 1.8$ GeV; and for π^-, $1.5 < E_\nu/\text{GeV} < 10$, $\theta_\mu < 25$ deg. and $W^{exp} < 1.8$ GeV. The restrictions to relatively low values of the invariant mass imply a more prominent contribution of the Δ resonance, while the restrictions to forward angles imply focusing, on average, on smaller values of the transferred energy and momentum, where nuclear effects are more important.

In Figure 11, we show results for CC neutrino-induced π^+ and antineutrino-induced π^0 production. For the neutrino CC1π^+ channel, two experimental datasets are shown: one corresponding to single-pion events and another that includes events with one or more pions ($n\pi$). We observe a general good agreement with data for this channel using both models, though some overestimation is obtained for scattering angles between 5 and 10 deg.

In the antineutrino CC1π^0 channel, the SuSAv2-DCC results exhibit a similar lack of strength as observed for MiniBooNE in Figure 4, producing the EDRMF-Hybrid approach better agreement with data. This is in accordance with the DCC vs. Hybrid differences observed in Figures 2 and 10 for the free-nucleon case.

In the neutrino CC1π^0 channel, Figure 12, we observe an important underestimation of the data. In this case, also the EDRMF-Hybrid model underpredict the data. As mentioned for MiniBooNE, Figure 4, other processes not included in this analysis, such as pion rescattering effects, could help to explain these discrepancies. Nevertheless, it is worth mentioning that, for the antineutrino case, the EDRMF-Hybrid model produces a reasonable agreement with data at these kinematics. As discussed in [55], this is peculiar since ^{12}C is a symmetric nucleus. Based on isospin symmetry, the leading order difference between the neutrino and antineutrino case is then the change of sign of the vector-axial interference contribution. The inconsistency in the description of these data may hence point to large uncertainties in the axial nucleon-to-resonance transition form factors in the second resonance region [14,63].

Finally, for the antineutrino CC1π^- channel, Fig 13, we observe that the EDRMF-Hybrid agrees with the data reasonably well while SuSAv2-DCC underestimate them. It can be ascribed to the differences between DCC and Hybrid shown in Figures 2 and 10 for the free-nucleon case.

In general, when comparing the ratios between DCC and Hybrid results in Figure 10 for scattering off single-nucleons at MINERvA kinematics with the SuSAv2-DCC and EDRMF-Hybrid ones in Figures 11–13, the cross section per nucleon for a bound nucleon compared to a free one is reduced in both models. This reduction is found to be stronger in the SuSAv2 model than in the EDRMF. [1]

3.0.3. T2K

In this section, the results for CC1π^+ at T2K kinematics are shown. The target of the T2K experiment is C_8H_8. The normalized neutrino flux is shown in Figure 14. It peaks at around 0.6 GeV, covering an energy range similar to the MiniBooNE flux (Sect. 3.0.1). In this case, the restriction $W^{exp} < 2.0$ GeV is applied, so contributions from processes beyond the Δ region are not removed as was the case for the MiniBooNE data. However, the main contribution to the π^+ production cross section remains the delta resonance, especially since the T2K flux peaks at relatively low energy.

 doi:10.20944/preprints202602.1441.v1

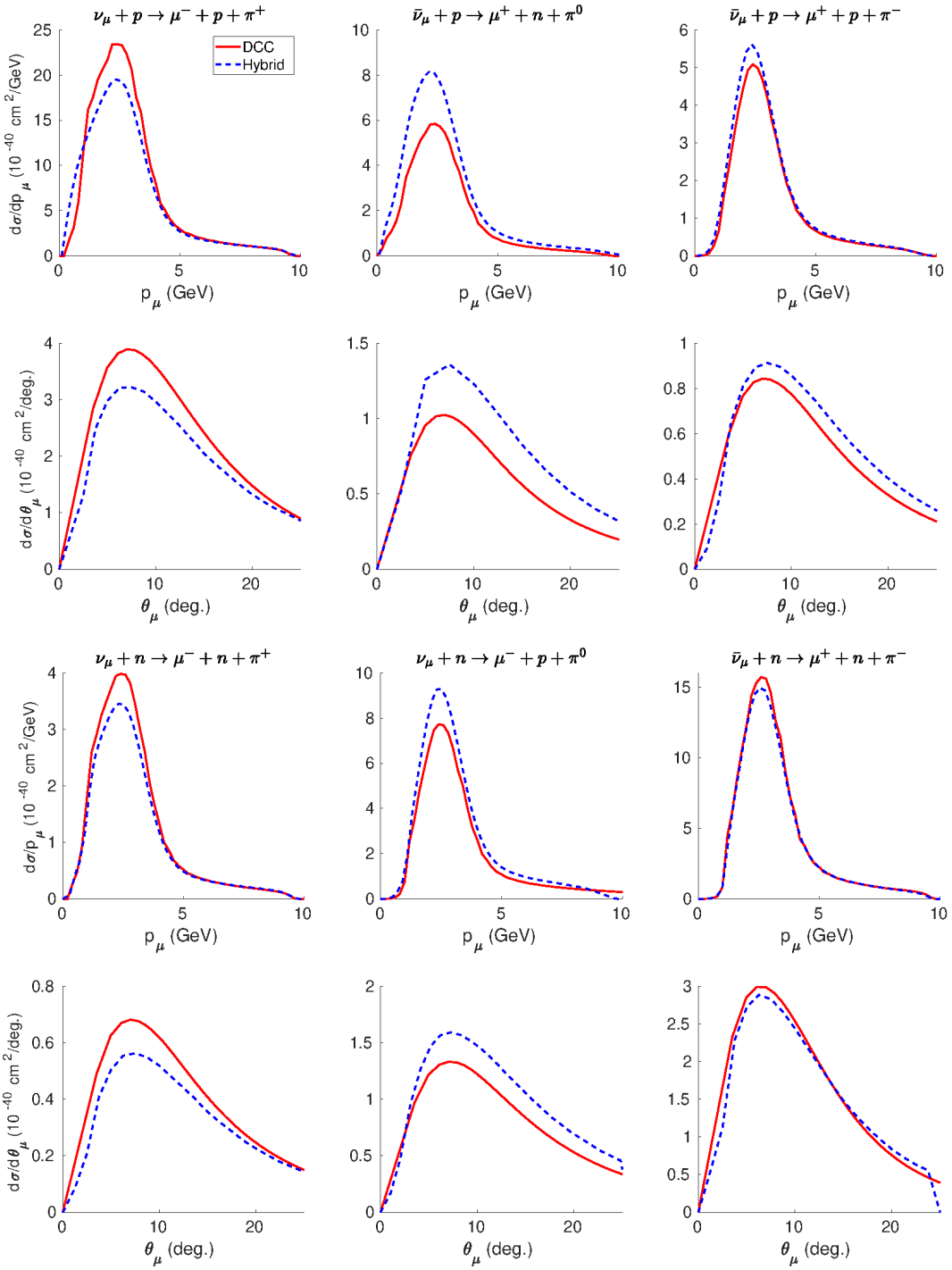

Figure 10. MINERνA flux-folded CC1π single-differential cross sections in terms of the muon momentum (top panels) and scattering angle (bottom panels) for different neutrino- and antineutrino-induced pion production scattering off single nucleons. (Left) π^+ processes for $1.5 < E_\nu/\text{GeV} < 10$ and $W^{exp} < 1.4$ GeV; (Center Top) $\bar{\nu}\pi^0$ processes for $1.5 < E_\nu/\text{GeV} < 10$ and $W^{exp} < 1.8$ GeV; (Center Bottom) $\nu\pi^0$ processes for $1.5 < E_\nu/\text{GeV} < 20$, $\theta_\mu < 25$ deg. and $W^{exp} < 1.8$ GeV; and (Right) π^- processes for $1.5 < E_\nu/\text{GeV} < 10$, $\theta_\mu < 25$ deg. and $W^{exp} < 1.8$ GeV.

 doi:10.20944/preprints202602.1441.v1

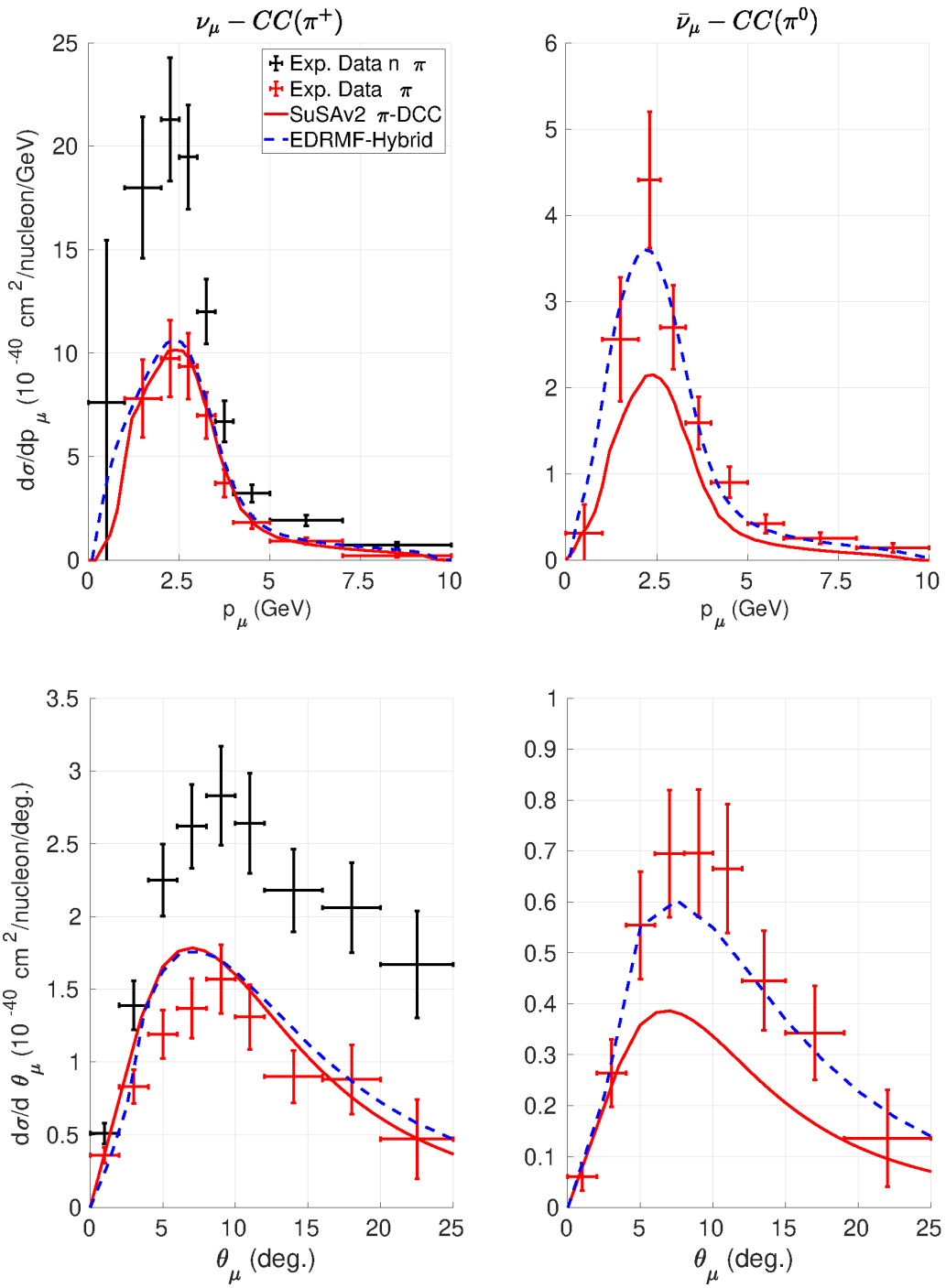

Figure 11. MINERvA flux-averaged CCπ^+ ν_μ-CH (left) and CC1π^0 $\bar{\nu}_\mu$-CH (right) differential cross sections as a function of the muon momentum (top) and the scattering angle (bottom) for multiple- (black data) and single-pion production (red data). The kinematical restrictions are (left) $W^{exp} < 1.4$ GeV, (right) $W^{exp} < 1.8$ GeV and $1.5 < E_\nu/\text{GeV} < 10$ for both cases. The experimental data points are taken from [60,64] .

 doi:10.20944/preprints202602.1441.v1

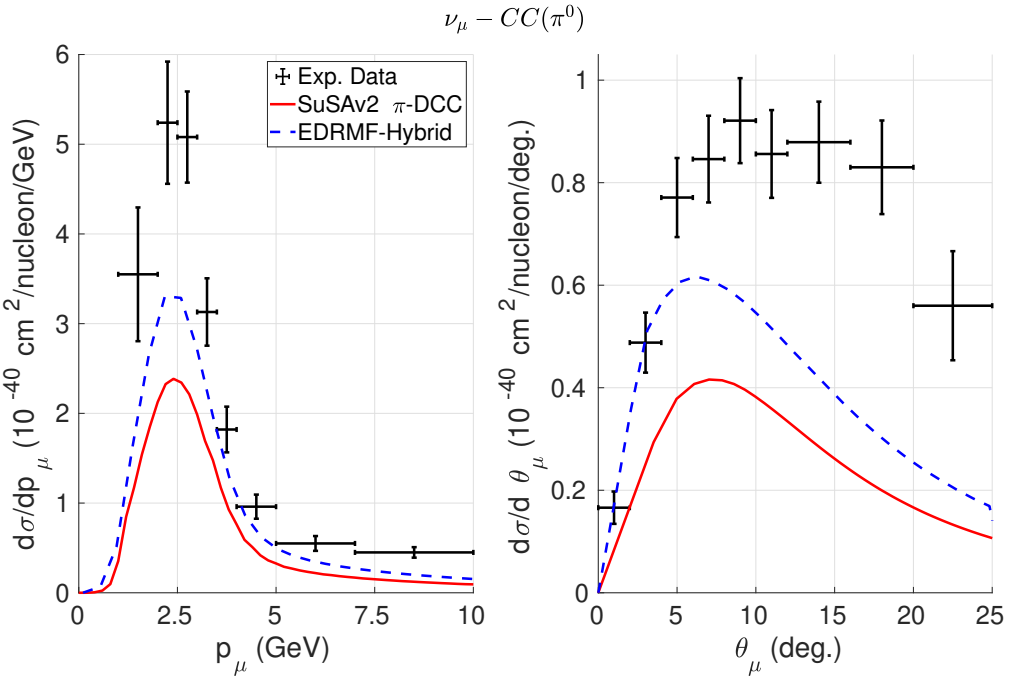

Figure 12. MINERvA flux-averaged CC1π^0 ν_μ-CH (left) differential cross sections as a function of the muon momentum (left) and the scattering angle (right). The kinematical restrictions are $1.5 < E_\nu/\text{GeV} < 20$, $\theta_\mu < 25$ deg. and $W^{exp} < 1.8$ GeV. The experimental data points are taken from [61].

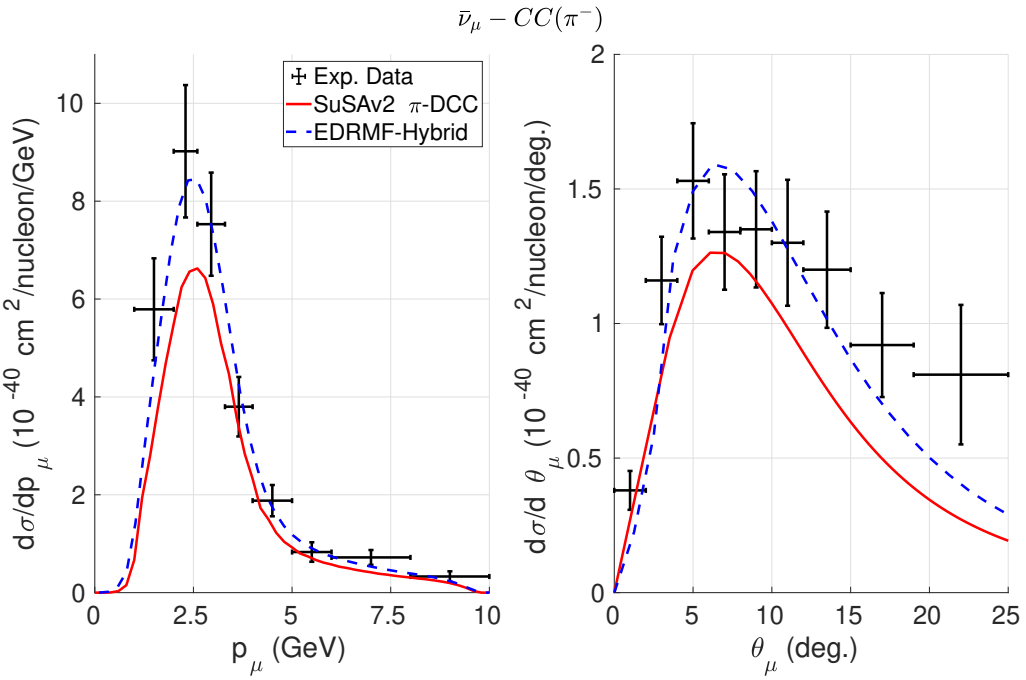

Figure 13. MINERvA flux-averaged CC1π^- $\bar{\nu}_\mu$-CH (left) differential cross sections as a function of the muon momentum (left) and the scattering angle (right). The kinematical restrictions are $1.5 < E_\nu/\text{ GeV} < 10$, $\theta_\mu < 25$ deg. and $W^{exp} < 1.8$ GeV. The experimental data points are taken from [62].

Figure 15 shows the flux-averaged ν_μ CC1π^+ double-differential cross section in bins of the muon scattering angle. The results are consistent with those shown for MiniBooNE. The predictions from EDRMF and SuSAv2 are close to the data and similar between them, with EDRMF producing smaller cross sections in general, which is consistent with the DCC and Hybrid differences observed in Figure 2.

 doi:10.20944/preprints202602.1441.v1

It is worth mentioning that, as in the previous cases, coherent pion production and pion rescattering effects are not taken into account by the models.

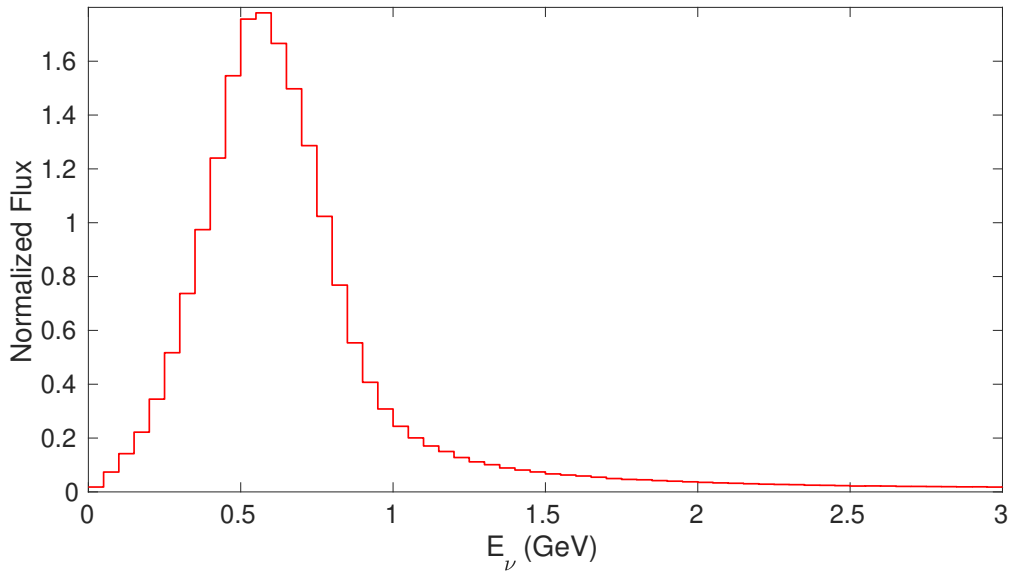

Figure 14. Normalized neutrino flux from T2K [65].

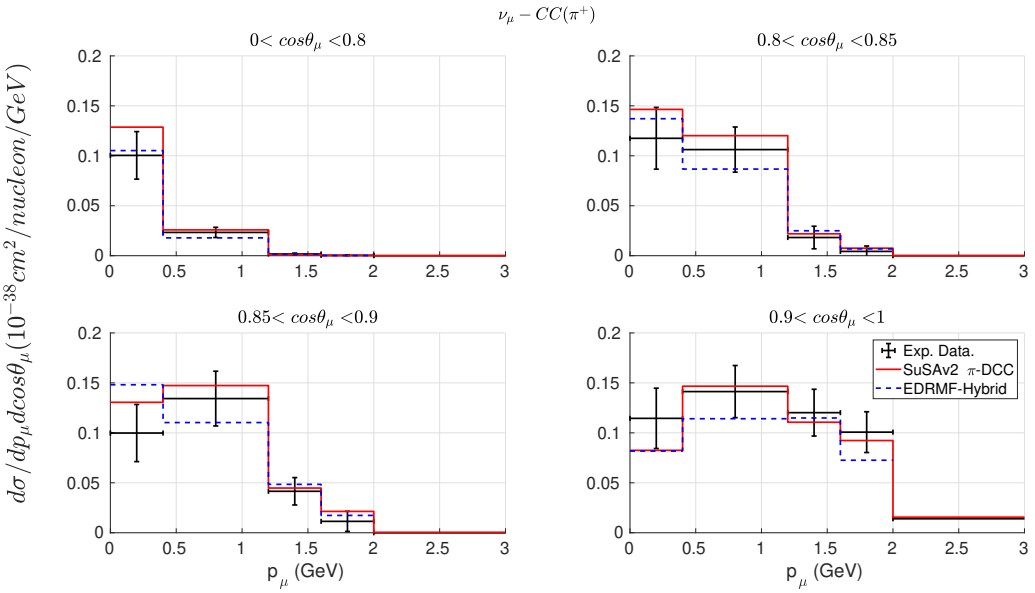

Figure 15. T2K flux-averaged CC1π^+ ν_μ-CH differential cross sections as a function of the muon energy in bins of the cosine of the scattering angle with $W^{exp} < 2.0$ GeV. The experimental T2K points are taken from [65].

4. Conclusions

This paper presents an extensive comparison of two different theoretical approaches with neutrino- and antineutrino-nucleus CC1π cross-section measurements. The single-pion production off the nucleon is described with the DCC [32–36] and the Hybrid [29,30] models. The DCC is incorporated into the SuSAv2-inelastic nuclear framework [37,52,53], while the Hybrid is integrated into an RDWIA approach; in particular, we use the EDRMF model to treat the distortion of the final nucleon [27], while the pion is described as a plane wave.

 doi:10.20944/preprints202602.1441.v1

In general, we found significant discrepancies between the two model predictions for all channels. In spite of the level of agreement observed in some figures, none of the models is able to provide a satisfactory description of all datasets.

When comparing our results with those of other theoretical approaches [18,30] and Monte Carlo event generators [59–62], we find similar pion-production contributions to other theoretical models, while generators predict larger cross sections for π^0 production results. In this context, the Monte Carlo intranuclear cascade effects (mainly pion rescattering effects in the nuclear medium, leading to pion charge exchanged) could improve our agreement with data, as observed in the Supplemental Material of [59], where these final-state interactions increase the CC1π^0 results. Note also the important discrepancies observed in this work for neutrino and antineutrino reactions in the π^0 channel between models and data, which may point to the importance of improvements in the modeling of axial contributions for CC1π interactions.

It is interesting that variations at the nucleon level, i.e., differences between DCC and Hybrid [Figures 2 and 10], are generally more relevant than those introduced by the nuclear model, i.e. differences due to the use of SuSAv2 or EDRMF. A slight general increase of the EDRMF results with respect to the SuSAv2 ones has also been observed, in particular at MINERvA kinematics. However, the ratio of cross sections per bound nucleon compared to the free nucleon is generally slightly smaller for SuSAv2 compared to the EDRMF, in particular in MINERvA kinematics.

The limits $Q^2 < 3$ GeV$^2/c^2$ and $W_x < 2.1$ GeV in the DCC model have little impact on the results presented here due to the experimental constraints. Nevertheless, it could be explored in the future via detailed studies with higher-energy neutrino experiments. Other recent and forthcoming datasets from different experiments, such as NOvA, T2K, MINERvA, and MicroBooNE [66–69], or on different targets, such as water [70] or argon [59], will also be analyzed in future works.

On the other hand, the recent implementation of superscaling and RDWIA models in neutrino event generators [71–74], such as GENIE or NEUT, mostly done for the QE and 2p2h regimes, will be extended in the future for the pion production and the full inelastic regime. This could allow us to apply intranuclear cascade effects (e.g., rescattering processes that can convert a π^+ into a π^0) to these analyses, with the possibility of having a more accurate description of final-state interaction effects, thus improving the agreement with data. The addition of other approaches for the single-nucleon inelastic structure functions, such as the MK model [39] will also be considered. Finally, the use of different nuclear potentials in the RDWIA framework will also be explored in further studies in a similar way to previous works [56,75], also bearing in mind more exclusive processes, i.e. cross-section measurements in terms of the kinematics of final-state pions and nucleons, which can improve nuclear model selection.

Data Availability Statement: No new data were created or analyzed in this study.

Acknowledgments: This work has received funding from the European Union's Horizon research and innovation programme under the Marie Skłodowska-Curie Actions (MSCA) HORIZON-MSCA-2023-SE-01-01 - MSCA Staff Exchanges 2023, Grant Agreement ID: 101183137 (JENNIFER3 project), and is partially supported by the Spanish Ministerio de Ciencia, Innovación y Universidades and ERDF (European Regional Development Fund) under contract PID2023-146401NB-I00, by the Junta de Andalucia (grants No. FQM160 and SOMM17/6105/UGR), by University of Tokyo ICRR's Inter-University Research Program FY2025 (Ref. 2025i-J-001), by the INFN under project Iniziativa Specifica NucSys and the University of Turin under Project BARM-RILO-24 (M.B.B.). J.G.R. was supported by a Contract PIF VI-PPITUS 2020 from the University of Seville (Plan Propio de Investigación y Transferencia). R.G.-J. was supported by projects PID2021-127098NA-I00 and RYC2022-035203-I funded by MCIN/AEI/10.13039/501100011033/FEDER and FSE+, UE; and by "Ayudas para Atracción de Investigadores con Alto Potencial-modalidad A" funded by VII PPIT-US. A.N. is supported by the Neutrino Theory Network (NTN) under Award Number DEAC02-07CH1135.

Conflicts of Interest: The authors declare no conflicts of interest.

 doi:10.20944/preprints202602.1441.v1

References

1. Taroni, A. Nobel Prize 2015: Kajita and McDonald. *Nature Physics* **2015**, *11*, 891–891. https://doi.org/10.1038/nphys3543.
2. Abe, K.; et al. Constraint on the matter–antimatter symmetry-violating phase in neutrino oscillations. *Nature* **2020**, *580*, 339–344, [arXiv:hep-ex/1910.03887]. [Erratum: Nature 583, E16 (2020)], https://doi.org/10.1038/s41586-020-2177-0.
3. Abubakar, S.; et al. Joint neutrino oscillation analysis from the T2K and NOvA experiments. *Nature* **2025**, *646*, 818–824, [arXiv:hep-ex/2510.19888]. https://doi.org/10.1038/s41586-025-09599-3.
4. Aguilar-Arevalo, A.A. The MiniBooNE Experiment, 2004. arXiv:hep-ex/0408074, https://doi.org/10.48550/arXiv.hep-ex/0408074.
5. MicroBooNE Collaboration. Website of the MicroBooNE Experiment(https://microboone.fnal.gov/), 2025. Last accessed January 2025.
6. T2K Collaboration. Website of the T2K Experiment(https://T2K-experiment.org/), 2025. Last accessed January 2025.
7. MINERvA Collaboration. Website of the MINERvA Experiment(https://minerva.fnal.gov/) , 2025. Last accessed January 2025.
8. NOvA Collaboration. Website of the NOvA Experiment(https://novaexperiment.fnal.gov/), 2025. Last accessed January 2025.
9. Abe, K.; et al. Hyper-Kamiokande Design Report **2018**. [arXiv:physics.ins-det/1805.04163].
10. Masud, M.; Bishai, M.; Mehta, P. Extricating New Physics Scenarios at DUNE with Higher Energy Beams. *Scientific Reports* **2019**, *9*, 352. https://doi.org/10.1038/s41598-018-36790-6.
11. Soderberg, M. ArgoNeuT: A Liquid Argon Time Projection Chamber Test in the NuMI Beamline, 2009. arXiv:0910.3433 [physics], https://doi.org/10.48550/arXiv.0910.3433.
12. Rein, D.; Sehgal, L.M. Neutrino-excitation of baryon resonances and single pion production. *Annals of Physics* **1981**, *133*, 79–153. https://doi.org/https://doi.org/10.1016/0003-4916(81)90242-6.
13. Fogli, G.; Nardulli, G. A new approach to the charged current induced weak one-pion production. *Nuclear Physics B* **1979**, *160*, 116–150. https://doi.org/10.1016/0550-3213(79)90233-5.
14. Lalakulich, O.; Paschos, E.A.; Piranishvili, G. Resonance production by neutrinos: The second resonance region. *Phys. Rev. D* **2006**, *74*, 014009. https://doi.org/10.1103/PhysRevD.74.014009.
15. Schreiner, P.A.; von Hippel, F. $\nu p \to \mu^- \Delta^{++}$ Comparison with Theory. *Physical Review Letters* **1973**, *30*, 339–342. https://doi.org/10.1103/PhysRevLett.30.339.
16. Matsui, K.; Sato, T.; Lee, T.S.H. Quark-hadron duality and parity violating asymmetry of electroweak reactions in the \ensuremath{\Delta} region. *Physical Review C* **2005**, *72*, 025204. Publisher: American Physical Society, https://doi.org/10.1103/PhysRevC.72.025204.
17. Hernández, E.; Nieves, J.; Vacas, M.J.V. Single π production in neutrino-nucleus scattering. *Phys. Rev. D* **2013**, *87*, 113009. https://doi.org/10.1103/PhysRevD.87.113009.
18. Martini, M.; Ericson, M. Inclusive and pion production neutrino-nucleus cross sections. *Phys. Rev. C* **2014**, *90*, 025501. https://doi.org/10.1103/PhysRevC.90.025501.
19. Yao, D.L.; Alvarez-Ruso, L.; Vicente Vacas, M. Neutral-current weak pion production off the nucleon in covariant chiral perturbation theory. *Physics Letters B* **2019**, *794*, 109–113. https://doi.org/https://doi.org/10.1016/j.physletb.2019.05.036.
20. Sogarwal, H.; Shukla, P. Coherent pion production in neutrino (anti-neutrino)-nucleus interaction. *Nuclear Physics A* **2022**, *1027*, 122494. https://doi.org/https://doi.org/10.1016/j.nuclphysa.2022.122494.
21. García-Marcos, J.; Franco-Munoz, T.; González-Jiménez, R.; Nikolakopoulos, A.; Jachowicz, N.; Udías, J.M. Towards a more complete description of nucleon distortion in lepton-induced single-pion production at low-Q^2. *Phys. Rev. C* **2024**, *109*, 024608. https://doi.org/10.1103/PhysRevC.109.024608.
22. Yan, Q.; Niewczas, K.; Nikolakopoulos, A.; González-Jiménez, R.; Jachowicz, N.; Lu, X.; Sobczyk, J.; Zheng, Y. The Ghent Hybrid model in NuWro: a new neutrino single-pion production model in the GeV regime. *Journal of High Energy Physics* **2024**, *2024*, 141. https://doi.org/10.1007/JHEP12(2024)141.
23. Horowitz, C.J.; Kim, H.; Murdock, D.P.; Pollock, S. Neutrino-nucleus quasifree neutral current reactions and the nucleon strange quark content. *Phys. Rev. C* **1993**, *48*, 3078–3087. https://doi.org/10.1103/PhysRevC.48.3078.
24. Alberico, W.M.; Barbaro, M.B.; Bilenky, S.M.; Giunti, J.A.C.C.; Maieron, C.; Guerra, E.M.d.; Udías, J.M. *Nucl. Phys. A* **1997**, *623*, 471.

 doi:10.20944/preprints202602.1441.v1

25. Nieves, J.; Simo, I.R.; Vacas, M.J.V. Inclusive charged-current neutrino-nucleus reactions. *Physical Review C* **2011**, *83*, 045501. https://doi.org/10.1103/PhysRevC.83.045501.
26. Rocco, N.; Nakamura, S.X.; Lee, T.S.H.; Lovato, A. Electroweak pion production on nuclei within the extended factorization scheme. *Phys. Rev. C* **2019**, *100*, 045503. https://doi.org/10.1103/PhysRevC.100.045503.
27. González-Jiménez, R.; Nikolakopoulos, A.; Jachowicz, N.; Udías, J.M. Nuclear effects in electron-nucleus and neutrino-nucleus scattering within a relativistic quantum mechanical framework. *Phys. Rev. C* **2019**, *100*, 045501. Publisher: American Physical Society, https://doi.org/10.1103/PhysRevC.100.045501.
28. Hernández, E.; Nieves, J.; Valverde, M. Weak pion production off the nucleon. *Phys. Rev. D* **2007**, *76*, 033005. https://doi.org/10.1103/PhysRevD.76.033005.
29. González-Jiménez, R.; Jachowicz, N.; Niewczas, K.; Nys, J.; Pandey, V.; Van Cuyck, T.; Van Dessel, N. Electroweak single-pion production off the nucleon: From threshold to high invariant masses. *Phys. Rev. D* **2017**, *95*, 113007. https://doi.org/10.1103/PhysRevD.95.113007.
30. González-Jiménez, R.; Niewczas, K.; Jachowicz, N. Pion production within the hybrid relativistic plane wave impulse approximation model at MiniBooNE and MINERvA kinematics. *Phys. Rev. D* **2018**, *97*, 013004. https://doi.org/10.1103/PhysRevD.97.013004.
31. Nikolakopoulos, A.; González-Jiménez, R.; Jachowicz, N.; Udías, J. Assessing the theory-data tension in neutrino-induced charged pion production: The effect of final-state nucleon distortion. *Physical Review D* **2023**, *107*. https://doi.org/10.1103/physrevd.107.053007.
32. Nakamura, S.; Kamano, H.; Sato, T. Dynamical coupled-channels model for neutrino-induced meson productions in resonance region. *Physical Review D* **2015**, *92*, 074024. https://doi.org/10.1103/PhysRevD.92.074024.
33. Nakamura, S.; Kamano, H.; Sato, T. Impact of final state interactions on neutrino-nucleon pion production cross sections extracted from neutrino-deuteron reaction data. *Physical Review D* **2019**, *99*, 031301. https://doi.org/10.1103/PhysRevD.99.031301.
34. Osaka University. Website of the ANL-Osaka DCC model(https://www.rcnp.osaka-u.ac.jp/ anl-osk/), 2021. Last accessed October 2023.
35. Sato, T.; Uno, D.; Lee, T.S.H. Dynamical model of weak pion production reactions. *Phys. Rev. C* **2003**, *67*, 065201. https://doi.org/10.1103/PhysRevC.67.065201.
36. Kamano, H.; Nakamura, S.X.; Lee, T.S.H.; Sato, T. Nucleon resonances within a dynamical coupled-channels model of πN and γN reactions. *Phys. Rev. C* **2013**, *88*, 035209. https://doi.org/10.1103/PhysRevC.88.035209.
37. Gonzalez-Rosa, J.; Megias, G.D.; Caballero, J.A.; Barbaro, M.B.; Franco-Patino, J.M. Superscaling in the resonance region for neutrino-nucleus scattering: The SuSAv2 dynamical coupled-channels model. *Phys. Rev. D* **2023**, *108*, 113008. https://doi.org/10.1103/PhysRevD.108.113008.
38. Isaacson, J.; Jay, W.; Lovato, A.; Machado, P.; Nikolakopoulos, A.; Rocco, N.; Steinberg, N. Single pion production and pion propagation in achilles. *Phys. Rev. D* **2026**, *113*, 036005, [arXiv:hep-ph/2508.19213]. https://doi.org/10.1103/13bh-22lm.
39. Kabirnezhad, M. Single pion production in neutrino-nucleon interactions. *Physical Review D* **2018**, *97*, 013002. https://doi.org/10.1103/PhysRevD.97.013002.
40. Hayato, Y.; Pickering, L. The NEUT neutrino interaction simulation program library. *Eur. Phys. J. ST* **2021**, *230*, 4469–4481, [arXiv:hep-ph/2106.15809]. https://doi.org/10.1140/epjs/s11734-021-00287-7.
41. Gonzalez-Rosa, J.; Megias, G.D.; Caballero, J.A.; Barbaro, M.B. Analysis of NOvA and MicroBooNE charged-current inclusive neutrino measurements within the SuSAv2 framework. *Phys. Rev. D* **2025**, *111*, 073002. https://doi.org/10.1103/PhysRevD.111.073002.
42. Nikolakopoulos, A.; González-Jiménez, R.; Niewczas, K.; Sobczyk, J.; Jachowicz, N. Modeling neutrino-induced charged pion production on water at T2K kinematics. *Phys. Rev. D* **2018**, *97*, 093008. https://doi.org/10.1103/PhysRevD.97.093008.
43. Donnelly, T.W.; Sick, I. Superscaling of inclusive electron scattering from nuclei. *Physical Review C* **1999**, *60*, 065502. https://doi.org/10.1103/PhysRevC.60.065502.
44. Amaro, J.E.; Barbaro, M.B.; Caballero, J.A.; González-Jiménez, R.; Megias, G.D.; Simo, I.R. Electron- versus neutrino-nucleus scattering. *Journal of Physics G: Nuclear and Particle Physics* **2020**, *47*, 124001. Publisher: IOP Publishing, https://doi.org/10.1088/1361-6471/abb128.
45. Amaro, J.E.; Barbaro, M.B.; Caballero, J.A.; Donnelly, T.W.; Gonzalez-Jimenez, R.; Megias, G.D.; Simo, I.R. Neutrino-nucleus scattering in the SuSA model. *Eur. Phys. J. ST* **2021**, *230*, 4321–4338. _eprint: 2106.02857, https://doi.org/10.1140/epjs/s11734-021-00289-5.

 doi:10.20944/preprints202602.1441.v1

46. Megias, G.; Amaro, J.; Barbaro, M.; Caballero, J.; Donnelly, T. Inclusive electron scattering within the SuSAv2 meson-exchange current approach. *Physical Review D* **2016**, *94*, 013012. https://doi.org/10.1103/PhysRevD.94.013012.
47. Megias, G.D.; Amaro, J.E.; Barbaro, M.B.; Caballero, J.A.; Donnelly, T.W.; Simo, I.R. Charged-current neutrino-nucleus reactions within the superscaling meson-exchange current approach. *Phys. Rev. D* **2016**, *94*, 093004. Publisher: American Physical Society, https://doi.org/10.1103/PhysRevD.94.093004.
48. Megias, G.D.; Barbaro, M.B.; Caballero, J.A.; Amaro, J.E.; Donnelly, T.W.; Simo, I.R.; Orden, J.W.V. Neutrino–oxygen CC0$\uppi$ scattering in the SuSAv2-MEC model. *J. Phys. G: Nucl. Part. Phys.* **2018**, *46*, 015104. Publisher: IOP Publishing, https://doi.org/10.1088/1361-6471/aaf3ae.
49. Megias, G.D.; Barbaro, M.B.; Caballero, J.A.; Dolan, S. Analysis of the MINERvA antineutrino double-differential cross sections within the SuSAv2 model including meson-exchange currents. *Phys. Rev. D* **2019**, *99*, 113002. https://doi.org/10.1103/PhysRevD.99.113002.
50. Megias, G.; Donnelly, T.; Moreno, O.; Williamson, C.; Caballero, J.; González-Jiménez, R.; De Pace, A.; Barbaro, M.; Alberico, W.; Nardi, M.; et al. Meson-exchange currents and quasielastic predictions for charged-current neutrino- C 12 scattering in the superscaling approach. *Physical Review D* **2015**, *91*, 073004. https://doi.org/10.1103/PhysRevD.91.073004.
51. Gonzaléz-Jiménez, R.; Megias, G.D.; Barbaro, M.B.; Caballero, J.A.; Donnelly, T.W. Extensions of Superscaling from Relativistic Mean Field Theory: the SuSAv2 Model. *Phys. Rev. C* **2014**, *90*, 035501. _eprint: 1407.8346, https://doi.org/10.1103/PhysRevC.90.035501.
52. Gonzalez-Rosa, J.; Megias, G.; Caballero, J.; Barbaro, M. SuSAv2 model for inelastic neutrino-nucleus scattering. *Physical Review D* **2022**, *105*, 093009. https://doi.org/10.1103/PhysRevD.105.093009.
53. Megias, G.D. Charged-current neutrino interactions with nucleons and nuclei at intermediate energies (PhD thesis), 2017.
54. Barbaro, M.B.; Caballero, J.A.; Donnelly, T.W.; Maieron, C. Inelastic electron-nucleus scattering and scaling at high inelasticity. *Physical Review C* **2004**, *69*, 035502. https://doi.org/10.1103/PhysRevC.69.035502.
55. Nikolakopoulos, A. Towards a more complete description of final-state interactions in electroweak single pion production off atomic nuclei (PhD Thesis), 2021.
56. González-Jiménez, R.; et al. Constraints in modeling the quasielastic response in inclusive lepton-nucleus scattering. *Phys. Rev. C* **2020**, *101*, 015503. Publisher: American Physical Society, https://doi.org/10.1103/PhysRevC.101.015503.
57. Aguilar-Arevalo, A.; et al. Measurement of neutrino-induced charged-current charged pion production cross sections on mineral oil at $E_\nu \sim 1$ GeV. *Phys. Rev. D* **2011**, *83*, 052007. https://doi.org/10.1103/PhysRevD.83.052007.
58. Aguilar-Arevalo, A.A.; et al. Measurement of ν_μ-induced charged-current neutral pion production cross sections on mineral oil at $E_\nu \in 0.5 - 2.0$ GeV. *Phys. Rev. D* **2011**, *83*, 052009. https://doi.org/10.1103/PhysRevD.83.052009.
59. Abratenko, P.; et al. Measurement of the differential cross section for neutral pion production in charged-current muon neutrino interactions on argon with the MicroBooNE detector. *Phys. Rev. D* **2024**, *110*, 092014. https://doi.org/10.1103/PhysRevD.110.092014.
60. McGivern, C.L.; et al. Cross sections for ν_μ and $\overline{\nu}_\mu$ induced pion production on hydrocarbon in the few-GeV region using MINERvA. *Phys. Rev. D* **2016**, *94*, 052005. https://doi.org/10.1103/PhysRevD.94.052005.
61. Altinok, O.; et al. Measurement of ν_μ charged-current single π^0 production on hydrocarbon in the few-GeV region using MINERvA. *Phys. Rev. D* **2017**, *96*, 072003. https://doi.org/10.1103/PhysRevD.96.072003.
62. Le, T.; et al. Measurement of $\overline{\nu}_\mu$ charged-current single π^- production on hydrocarbon in the few-GeV region using MINERvA. *Phys. Rev. D* **2019**, *100*, 052008. https://doi.org/10.1103/PhysRevD.100.052008.
63. Sato, T. Neutrino–nucleon reactions in resonance region. *Eur. Phys. J. ST* **2021**, *230*, 4409–4418. https://doi.org/10.1140/epjs/s11734-021-00284-w.
64. Updated 1Pi production data. MINERvA Collaboration. https://minerva.fnal.gov/wp-content/uploads/2017/03/Updated_1pi_data.pdf. Last accessed: January 2026.
65. Abe, K.; et al. Measurement of the muon neutrino charged-current single π^+ production on hydrocarbon using the T2K off-axis near detector ND280. *Phys. Rev. D* **2020**, *101*, 012007. https://doi.org/10.1103/PhysRevD.101.012007.
66. Abubakar, S.; et al. Measurement of π^0 Production in $\bar{\nu}_\mu$ Charged-Current Interactions in the NOvA Near Detector **2025**. [arXiv:hep-ex/2511.05807].

 doi:10.20944/preprints202602.1441.v1

67. Abe, K.; et al. First Measurement of the Electron-Neutrino Charged-Current Pion Production Cross Section on Carbon with the T2K Near Detector. *Phys. Rev. Lett.* **2025**, *135*, 151802, [arXiv:hep-ex/2505.00516]. https://doi.org/10.1103/klhv-7t6h.
68. Lozano, A.; et al. Measurement of charged-current ν_μ and $\bar{\nu}_\mu$ cross sections on hydrocarbon in a shallow inelastic scattering region **2025**. [arXiv:hep-ex/2503.20043].
69. Abratenko, P.; et al. First Measurement of ν_e and $\bar{\nu}_e$ Charged-Current Single Charged-Pion Production Differential Cross Sections on Argon Using the MicroBooNE Detector. *Phys. Rev. Lett.* **2025**, *135*, 061802, [arXiv:hep-ex/2503.23384]. https://doi.org/10.1103/sfrz-c8m9.
70. Abe, K.; et al. First measurement of the muon neutrino charged current single pion production cross section on water with the T2K near detector. *Phys. Rev. D* **2017**, *95*, 012010. https://doi.org/10.1103/PhysRevD.95.012010.
71. Dolan, S.; Megias, G.D.; Bolognesi, S. Implementation of the SuSAv2-meson exchange current 1p1h and 2p2h models in GENIE and analysis of nuclear effects in T2K measurements. *Phys. Rev. D* **2020**, *101*, 033003, [arXiv:hep-ex/1905.08556]. https://doi.org/10.1103/PhysRevD.101.033003.
72. Papadopoulou, A.; et al. Inclusive Electron Scattering And The GENIE Neutrino Event Generator. *Phys. Rev. D* **2021**, *103*, 113003, [arXiv:nucl-th/2009.07228]. https://doi.org/10.1103/PhysRevD.103.113003.
73. McKean, J.; González-Jiménez, R.; Kabirnezhad, M.; Udías, J.M.; Uchida, Y. Implementation of a relativistic distorted wave impulse approximation model into the NEUT event generator. *Phys. Rev. D* **2025**, *112*, 032009. https://doi.org/10.1103/f7x5-snmz.
74. Khachatryan, M.; et al. Electron-beam energy reconstruction for neutrino oscillation measurements. *Nature* **2021**, *599*, 565–570. https://doi.org/10.1038/s41586-021-04046-5.
75. Franco-Patino, J.M.; González-Jiménez, R.; Dolan, S.; Barbaro, M.B.; Caballero, J.A.; Megias, G.D.; Udias, J.M. Final state interactions in semi-inclusive neutrino-nucleus scattering: Applications to the T2K and MINERνA experiments. *Phys. Rev. D* **2022**, *106*, 113005. https://doi.org/10.1103/PhysRevD.106.113005.